UNIVERSITY *of York*

This is a repository copy of *Ozone production by an He+O2 radio-frequency atmospheric pressure plasma jet driven by tailored voltage waveforms*.

Article:

Harris, Benjamin, Dedrick, James Peter orcid.org/0000-0003-4353-104X, Niemi, Kari orcid.org/0000-0001-6134-1974 et al. (1 more author) (2024) Ozone production by an He+O2 radio-frequency atmospheric pressure plasma jet driven by tailored voltage waveforms. Plasma Sources Science and Technology. 075020. ISSN 0963-0252

https://doi.org/10.1088/1361-6595/ad6587

White Rose
university consortium
Universities of Leeds, Sheffield & York

eprints@whiterose.ac.uk
https://eprints.whiterose.ac.uk/

PAPER • OPEN ACCESS

Ozone production by an He+O$_2$ radio-frequency atmospheric pressure plasma jet driven by tailored voltage waveforms

View the article online for updates and enhancements.

Ozone production by an He+O$_2$ radio-frequency atmospheric pressure plasma jet driven by tailored voltage waveforms

Benjamin Harris[*] ⓘ**, James P Dedrick**ⓘ**, Kari Niemi**ⓘ
and Erik Wagenaarsⓘ

York Plasma Institute, School of Physics, Engineering and Technology, University of York, Heslington, York YO10 5DD, United Kingdom

E-mail: ben.harris@oxinst.com and benjamin.harris@york.ac.uk

CrossMark

Abstract

Atmospheric pressure plasma jets are efficient sources of reactive oxygen and nitrogen species with potential applications in medicine, materials processing, green industry and agriculture. However, selective control over the production of reactive species presents an ongoing challenge and a barrier to the widespread uptake of these devices in applications. This study therefore investigates the production of ozone by a radio-frequency plasma jet driven with tailored voltage waveforms composed of up to five consecutive harmonics, with a fundamental frequency of 13.56 MHz. The plasma is supplied with helium with small admixtures (0.1%–1.0%) of oxygen gas. The ozone density in the far effluent is measured with Fourier transform infrared spectroscopy and the gas temperature in the plasma channel is determined with optical emission spectroscopy. Voltage waveform tailoring is found to enhance the ozone density in the far effluent of the plasma jet in comparison to operation with single-frequency voltage waveforms. Increasing the number of applied harmonics in the driving voltage waveform for a fixed peak-to-peak voltage enhances the ozone density but significantly increases the gas temperature within the plasma channel. Meanwhile, increasing the number of applied harmonics while maintaining a constant RF power deposition allows the density of ozone in the effluent to be increased by up to a factor of 4 relative to single-frequency operation, up to a maximum density of 5.7×10^{14} cm^{-3}, without any significant change to the gas temperature. This work highlights that tailored voltage waveforms can be used to control the density of ozone delivered through the plasma effluent, marking an important step towards realising the potential of these plasmas for applications.

Keywords: tailored voltage waveforms, atmospheric pressure plasma jet, ozone production, plasma chemistry

---

[*] Author to whom any correspondence should be addressed.

1. Introduction

Non-thermal, atmospheric pressure plasmas have garnered considerable interest in recent years as efficient sources of reactive oxygen and nitrogen species (RONS), with applications spanning the fields of medicine, materials processing, green industry, and agriculture [1–5]. In particular, atmospheric pressure plasma jets (APPJs) are versatile instruments that are operated in open air and at close to room temperature for the direct delivery of RONS to a substrate [6–15]. One such RONS is ozone (O_3). Ozone is an effective antimicrobial agent, used in biomedicine [16] and in the food industry [17]. Additionally, ozone generated by dielectric barrier discharge (DBD) reactors plays an essential role in plasma-based water treatment [18, 19].

APPJs are often operated with a helium feed gas, due in part to its high thermal conductivity that mitigates thermal instabilities [20]. RONS are generated in controllable amounts by introducing small admixtures of molecular gases, such as oxygen, nitrogen, or water vapour [21–31]. The plasma chemistry is heavily influenced by the electron dynamics; electrons accelerated by the electric field collide with neutrals, generating radical or metastable species through dissociation and excitation. In turn, these species form longer-lived RONS, including ozone, which are carried through the plasma effluent. Thus, the densities of ozone and other long-lived RONS are largely dictated by the electron energy distribution function (EEDF).

Capacitively-coupled APPJs are typically driven by radio-frequency (RF) voltage waveforms with low voltage amplitudes (a few hundred volts) and a single applied frequency of 13.56 MHz [9–11]. Operation in this manner produces a homogeneous glow discharge known as the Ω-mode, defined by volumetric electron heating [32]. In the Ω-mode, a high drift electric field within the plasma bulk triggers ionisation maxima during times of sheath expansion and collapse [33]. The gas temperature in the Ω-mode is relatively low, typically close to room temperature [34]. If the amplitude of the driving voltage waveform is increased, the mode of power coupling changes and the plasma transitions into the Penning-mode [35, 36]. Penning ionisation becomes the dominant ionisation process in this mode, with ionisation maxima occurring within the sheaths at times of maximum sheath expansion [33, 35]. The Ω-mode and Penning-mode are sometimes referred to as the α-mode and γ-mode, respectively, due to similarities with the low pressure plasma modes of the same name [37, 38]. Increasing the driving voltage amplitude eventually transitions the discharge into a constricted mode, characterised by filamentary behaviour. In this mode, ionisation is confined to the strongly contracted sheath regions [39, 40]. Operating APPJs in the constricted mode is best avoided, as the high gas temperature and current density pose a risk of thermal damage to the device and/or substrate [11, 38].

In the Ω-mode and the Penning-mode, electron power absorption is symmetrical in both space and time within the RF period. The extent to which the EEDF can be controlled in these modes is therefore limited, prompting research into alternative RF voltage waveforms as a means of controlling the plasma chemistry. This would allow the plasma chemistry to be tailored conveniently, without the need for physical adjustments to the plasma source. One prospect is dual-frequency operation, where a plasma is driven with a voltage waveform containing one low-frequency and one high-frequency component [41–50]. Further development of this method arose from the use of tailored voltage waveforms (TVWs), a technique originally applied to low pressure plasma sources [51–56]. TVWs are generated as a finite Fourier series of N consecutive harmonics of a fundamental frequency, f_0. Common types of TVW include the 'peaks' waveform, with its inverse known as the 'valleys' waveform [57]. Similarly, there is the 'sawtooth-up' waveform and its inverse counterpart, the 'sawtooth-down' waveform [57].

At atmospheric pressure, Gibson *et al* found that TVWs break the spatio-temporal symmetry of electron power absorption and allow the EEDF of an APPJ to be tailored directly [58]. By comparing phase-resolved optical emission with the results of a particle-in-cell code with Monte Carlo treatment of collisional processes (PIC/MCC), they showed that sawtooth waveforms induce temporally asymmetric electron heating, with maxima found at only one time within the RF cycle. Meanwhile, peaks and valleys waveforms induce electron heating that is asymmetric in both time and space, with maxima restricted to one electrode and at one time within the RF cycle. Hence, the EEDF is strongly influenced by the electron heating confinement induced by both types of waveform [58]. Following this, Korolov *et al* found that the spatio-temporally asymmetric electron heating of the peaks waveform stems from a short sheath collapse occurring only at the powered electrode [59]. The flux of ions to the powered electrode is compensated by the formation of a strong electric field. This causes electrons to be strongly accelerated close to the powered electrode, resulting in highly localised power absorption. Using a valleys waveform reverses the geometry of this process, instead localising power absorption to the region near the grounded electrode [60]. Confining the electron heating to small regions of space and time in this way enhances the high energy tail of the EEDF, allowing reactive species to be generated with increased efficiency and at higher densities when compared with single-frequency operation [61]. Another important aspect of TVW operation is that increasing the number of applied harmonics in the driving voltage waveform enhances the asymmetry of power absorption. Korolov *et al* demonstrated that increasing the number of harmonics can be used to optimise the densities of reactive species, including metastable helium, atomic nitrogen, and atomic oxygen [60, 62].

Overall, the effects of TVW operation on the electron dynamics and the production of radicals and metastables in the plasma channel of APPJs now appear well-understood. However, the extent to which TVWs influence longer-lived RONS in the effluent, such as ozone, has not yet been explored in detail. Nor has the impact of TVWs on the gas temperature of an APPJ been investigated. These two aspects are crucial when considering the safe and effective application of TVW-driven APPJs in medicine or industry. With this in mind, this work investigates the influence of TVWs on the density of ozone in the far effluent of an APPJ.

Ozone is chosen as a characteristic example of a long-lived RONS that is present in the effluent of APPJs. The authors acknowledge that a DBD reactor supplied with oxygen or air is generally the preferred source of ozone for industrial wastewater treatment and similar volumetric applications, due to the scalability and efficiency of DBD systems compared to APPJs [63]. APPJs are instead useful for convenient targeted delivery of reactive plasma-chemical mixtures, and for the synergistic effects that can be achieved between individual RONS, including ozone.

The paper is structured as follows: section 2 describes the APPJ design, the voltage waveform tailoring apparatus, and the spectroscopic techniques used to measure the ozone density and gas temperature. Section 3 presents the results of the investigations into the dependence of the ozone density in the far effluent on the type of TVW, the O_2 admixture concentration, the peak-to-peak voltage, and the number of applied voltage harmonics.

2. Experimental methods

2.1. Plasma source

The plasma source is an APPJ that has been established in previous works [64, 65]. A schematic of the device is shown in figure 1.

The plane-parallel stainless steel electrode assembly is designed to be similar to that of the COST-Jet [11] and its precursor, the μAPPJ [10]. The electrode gap of 1 mm is the same, the length of 24 mm comparable, but the width of 8.6 mm much larger than the original 1 mm. This design offers a longer absorption beam path for previous measurements of atomic oxygen and nitrogen ground state densities by vacuum ultraviolet spectroscopy at the DESIRS beamline of the SOLEIL synchrotron facility [64–66]. As such, the APPJ has a smaller surface-to-volume ratio and an appreciably larger plasma volume than the COST-Jet and μAPPJ. The electrodes are sealed between two circular MgF_2 windows. The grounded electrode also forms the housing of the plasma source. Mass flow controllers (MFCs) supply the APPJ with 5 slm of helium and admixtures of O_2 in the range of 0.1%–1.0%. The O_2 admixture concentration is chosen to maximise the range of applied voltage harmonics that can be investigated under equivalent conditions. The gas outlet of the APPJ is sealed to allow isolated measurements of the plasma effluent.
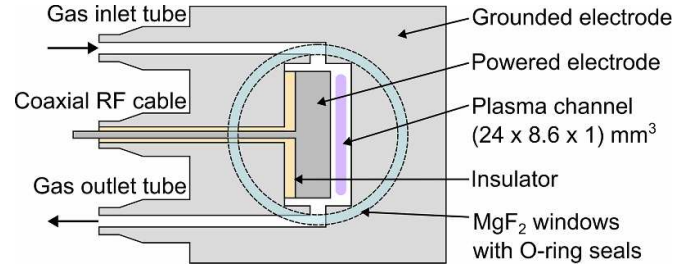

Figure 1. Schematic cross-section of the atmospheric pressure plasma source.

2.2. TVWs

TVWs are generated as a sum of N consecutive harmonics with fundamental frequency $f_0 = 13.56$ MHz. 'Peaks'- and 'valleys'-type waveforms are generated according to [67]

$$\phi(t) = \sum_{k=1}^{N} \phi_k \cos\left(2\pi k f_0 t + \theta_k\right),\tag{1}$$

where $\phi(t)$ is the voltage amplitude at time t. ϕ_k and θ_k are the amplitude and phase angle of individual harmonic k, respectively. ϕ_k is set according to

$$\phi_k = \phi_{pp}\frac{2\left(N-k+1\right)}{\left(N+1\right)^2},\tag{2}$$

in which ϕ_{pp} is the peak-to-peak voltage of the waveform. Setting all phase angles to zero produces a peaks waveform, while changing the phase angles of all even harmonics to $\theta_k = \pi$ yields a valleys waveform. Example peaks waveforms are shown in figure 2(a). 'Sawtooth'-type waveforms are generated with a separate function [68]:

$$\phi(t) = \phi_0 \sum_{k=1}^{N} \frac{N-k+1}{N} \cos\left(2\pi k f_0 t + \theta_k\right),\tag{3}$$

where the voltage amplitude prefactor ϕ_0 is set to give the desired peak-to-peak voltage. Setting all the phase angles to $\theta_k = \pi/2$ produces a sawtooth-up waveform, while a sawtooth-down waveform is attained by changing all the phase angles to $\theta_k = 3\pi/2$. Example sawtooth-up waveforms are shown in figure 2(b).

2.3. Description of the experimental setup

Figure 3 shows the full experimental setup, including diagnostics and the equipment used to drive the APPJ with TVWs.

The RF power, current, and applied voltage waveforms are measured with a Vigilant Power Monitor (VPM-13.56-1000-1 F-1 M, SOLAYL SAS, rating: 1 kW), abbreviated to VPM [69]. The plasma power, P_{RF}, is defined as the RF power deposited into the plasma. For a given voltage waveform, P_{RF}
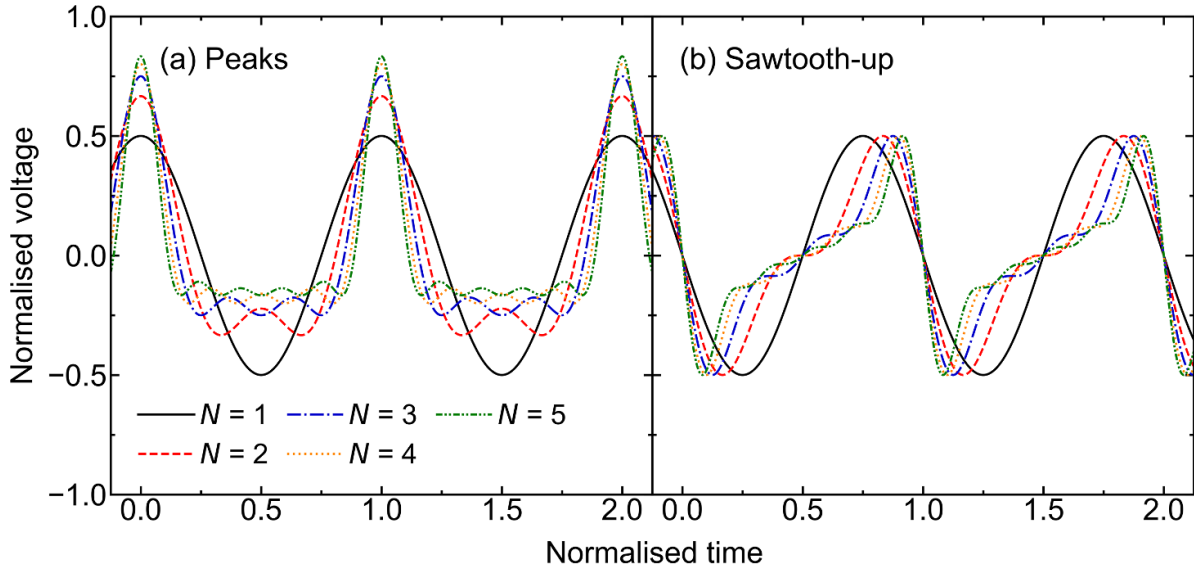
Figure 2. Representative (a) peaks and (b) sawtooth-up voltage waveforms for $N = 1$ to $N = 5$ consecutive harmonics, generated according to equations (1) and (3), respectively. The voltage axis is normalised to ϕ_{pp}. The time axis is normalised to the RF period, $1/f_0$.
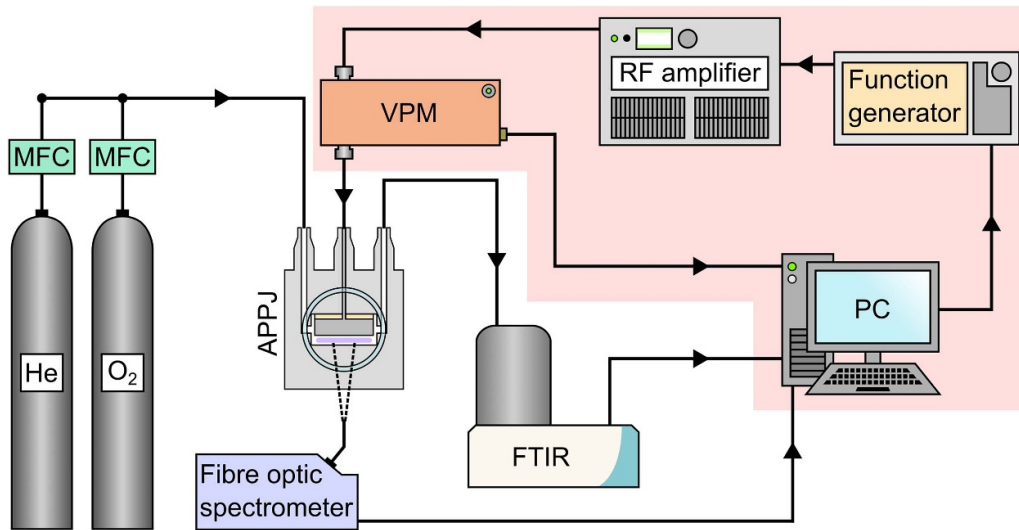

Figure 3. Schematic of the experimental setup. The shaded region shows the iterative feedback loop used to achieve a desired voltage waveform shape. For single frequency measurements this loop is replaced with an RF power generator and an impedance matching network. VPM: vigilant power monitor, MFC: mass flow controller.

is determined by taking the difference between the total measured RF power with and without plasma at a constant current, to account for all parasitic power losses in the system [70]. For single-frequency operation (i.e. $N = 1$), the APPJ is powered with a 13.56 MHz RF power generator (RFG 150–13, Coaxial Power Systems) through an L-type impedance matching network unit (MMN 150–13, Coaxial Power Systems), with the VPM connected in series directly before the APPJ. For operation with TVWs (i.e. $N > 1$), an iterative feedback loop is implemented to achieve the desired waveform shapes. This system was described by Doyle *et al* [56], and a summary is provided here. An initial seed waveform is set with

an arbitrary function generator (33 621A, Keysight) and amplified with a broadband power amplifier (GN500D, PRANA R&D, rating: 500 W), before being applied to the APPJ. The VPM is connected directly before the APPJ. The type of TVW, the peak-to-peak voltage and the number of applied harmonics are set on the PC with a companion software suite to the VPM (Vigilant RF lab, SOLAYL SAS). The software then reads the applied waveform from the VPM and modifies the harmonics, phases and amplitudes of the seed waveform in the arbitrary function generator. This process is iterated until the target waveform is achieved, and then stopped for taking measurements. The amplitude and shape of the applied
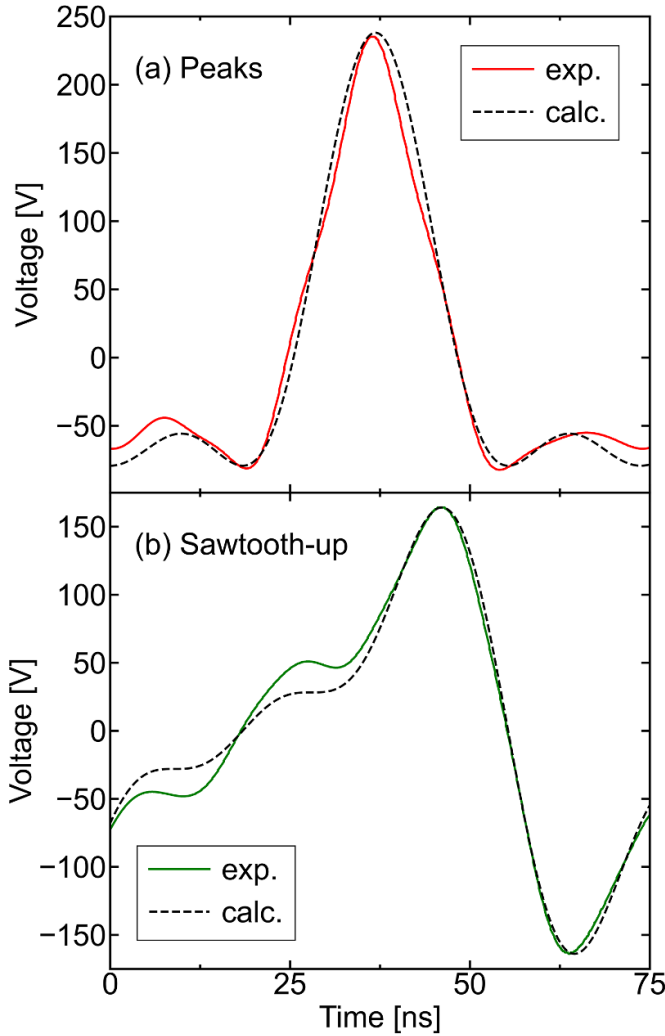
Figure 4. Comparison between measured applied voltage waveform and targeted waveform: (a) peaks and (b) sawtooth-up, for $N = 3$ harmonics according to equations (1) and (3). The feed gas is He+O$_2$ (0.1%).

voltage waveforms were previously found to be within 5% of the targeted waveforms [56]. Figure 4 shows representative examples of experimentally measured peaks and sawtooth-up voltage waveforms for $N = 3$ applied harmonics. To illustrate the degree of agreement, figure 4 also shows theoretical waveforms generated with equations (1) and (3), with the same peak-to-peak voltage as their measured equivalent.

2.4. Fourier transform infrared (FTIR) spectroscopy

The space- and time-averaged ozone density in the far effluent of the APPJ is measured by FTIR spectroscopy. The effluent gas mixture is piped through a 2 m long tube (perfluoroalkoxy material) into an optical multi-pass absorption gas cell (volume 2 L, absorption length 10 m) of a commercial Fourier transform spectrometer (Nicolet iS50, Thermo Fisher Scientific). The chosen spectral resolution is 4.0 cm^{-1}. A typical FTIR spectrum, from an average of 128 individual scans and after background subtraction, is shown in figure 5.
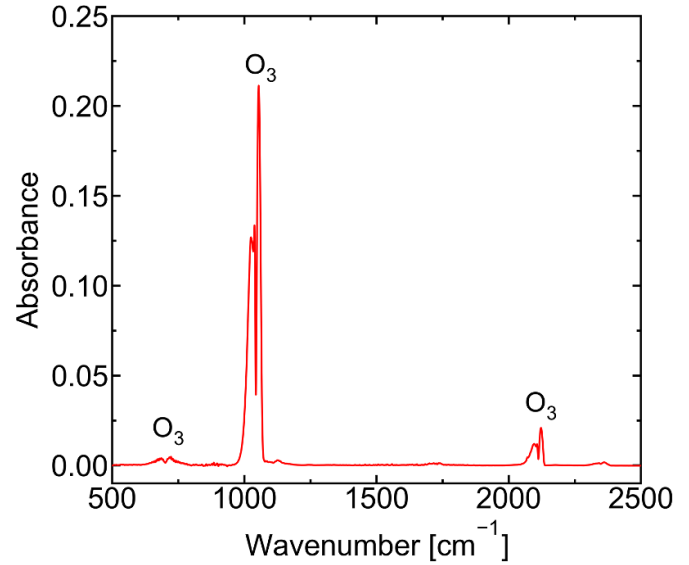

Figure 5. Measured FTIR absorption spectrum obtained in the far effluent of a He+O$_2$(0.5%) plasma, corresponding to an ozone density of 5.11×10^{14} cm^{-3}. Measurements are taken in optically thin conditions. Spectral structure explained in text.

As shown in figure 5, the electronic ground state of the ozone molecule exhibits an asymmetric top geometrical configuration with three fundamental modes: symmetric bending at $\nu_2 = 701$ cm^{-1}, asymmetric stretching at $\nu_3 = 1042$ cm^{-1}, and symmetric stretching at $\nu_1 = 1103$ cm^{-1} [71, 72]. The corresponding ro-vibrational bands appear in the measured absorbance spectrum, as well as the overtone and combination bands, e.g. $2\nu_3$ at 2084 cm^{-1} and $\nu_1 + \nu_3$ at 2110 cm^{-1} [71].

The data in the mid-infrared region between 550 cm^{-1} and 2200 cm^{-1} is analysed as follows. Assuming the gas mixture to be distributed homogeneously within the multi-pass cell, the optical absorbance is given by

$$A_{\text{int}}(\nu) = nd\sigma(\nu) = nd \sum_i \left[S_i \cdot f(\nu, \nu_i) \right], \tag{4}$$

where A_{int} is the measured absorbance integrated along absorption length d, n is the ozone density, and $\sigma(\nu)$ is the absorption cross-section of ozone at wavenumber ν. S_i is the line strength of transition i, centred at wavenumber ν_i, at 296 K, as the effluent gas is expected to relax to room temperature before reaching the multi-pass cell [20]. Line strengths and positions are taken from the HITRAN database [73]. Included transitions are restricted to those with a line strength above 10^{-22} cm^{-1} / (molec. $\cdot$ cm^{-2}), with the largest line strength in the range probed being 4.17×10^{-20} cm^{-1} / (molec. $\cdot$ cm^{-2}), centred at 1042 cm^{-1}. $f(\nu, \nu_i)$ is the line shape function of transition i at wavenumber ν. Since instrumental broadening is by far the dominant line broadening mechanism, we assume a common Gaussian line shape with 4.0 cm^{-1} full width at half maximum (FWHM) for all transitions. The theoretical absorbance spectrum is then calculated and numerically fitted to the measured spectra using a least squares fitting routine in order to determine the ozone

density. An uncertainty in the measured ozone densities of approximately $\pm 10\%$ is established, based on the standard deviation of the numerical fit and the reproducibility of the measurements.

2.5. Gas temperature from optical emission spectroscopy (OES)

The gas temperature within the core plasma of the APPJ is measured by OES. A fibre optic spectrograph (HR4000, Ocean Optics, spectral resolution: 0.03 nm) is used to measure the optical emission of molecular nitrogen through the $N_2(C^3\Pi_u - B^3\Pi_g)$ second positive system, which is collected from the centre of the plasma channel. No $N_2(C-B)$ emission is observed under standard operating conditions due to the sealed He+O_2 plasma environment. As such, small amounts of N_2 (up to 0.1%) are admixed into the feed gas before OES measurements are taken. The electrical characteristics of the discharge were found to be unaffected by this. OES measurements are performed separately to ozone density measurements to ensure that no trace N_2 is present to disrupt the oxygen plasma chemistry.

The rotational band of the $v' = 0 \rightarrow v'' = 0$ vibrational transition, centred near 337 nm, has the highest signal-to-noise ratio in the measurement range and is therefore chosen for analysis. The spectra show no overlap of the $(v = 0 \rightarrow 0)$ band with other spectral features. It is assumed that the rotational levels of the upper $N_2(C)$ state are in thermal equilibrium with the background gas; this is expected in atmospheric pressure helium discharges due to the short ro-translational relaxation time of $N_2(C)$ relative to the effective lifetime of the state [74, 75]. Thus, fitting the measurements with a simulated rotational spectrum allows the neutral gas temperature to be determined [76]. An example of a measured $N_2(C-B)$ $(v = 0 \rightarrow 0)$ spectrum and simulated fit are shown in figure 6. Measured spectra are fitted with a code used in previous studies [64, 77–81]. The simulation is modelled according to Herzberg [82], with rotational constants from Roux *et al* [83] and line strengths calculated from Kovács [84] and Schadee [85]. The resulting gas temperature readings have a characteristic uncertainty of ± 12 K. This value is calculated based only on the variation between repeat readings and the standard deviation between the model fit and experimental data.

3. Results and discussion

3.1. Influence of the O_2 admixture concentration

Figure 7 shows the measured ozone density in the far effluent as a function of the O_2 admixture for different types of TVW. The O_2 admixture concentration is varied from 0.2% to 1.0%. The peak-to-peak voltage is $\phi_{pp} = 420$ V. Each TVW is composed of $N = 3$ consecutive harmonics, as shown in figure 4. $N = 3$ harmonics is chosen as this generates a distinct shape for each type of TVW while still offering a reasonable operational range.

The density of ozone in the effluent increases linearly with the O_2 concentration for all four types of TVW. Both
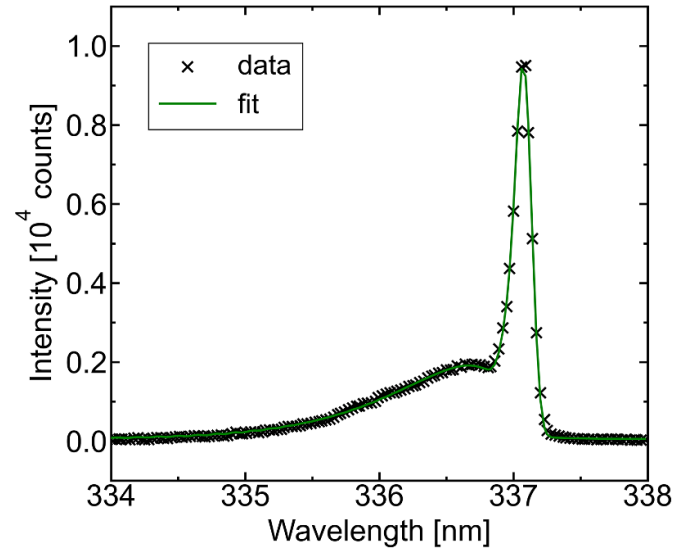

Figure 6. Measured optical emission spectrum and best fit of the $N_2(C^3\Pi_u - B^3\Pi_g)$ $(v = 0 \rightarrow 0)$ rotational band for a He+O_2 plasma with trace amounts of N_2. $\phi_{pp} = 315$ V.
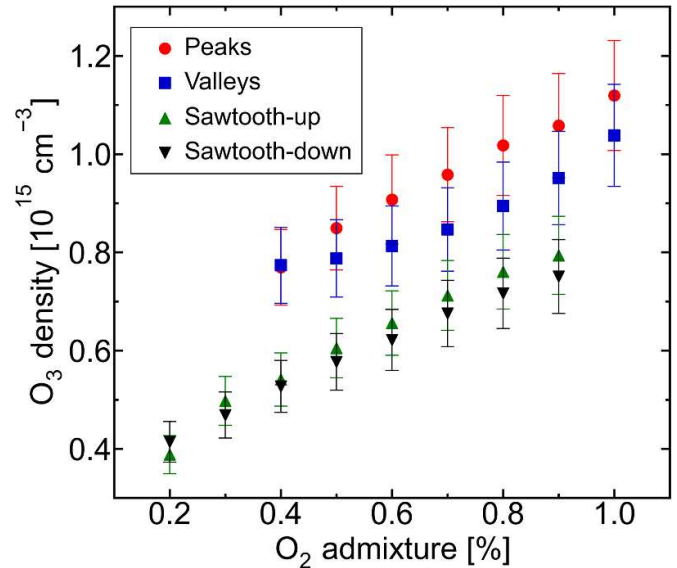
Figure 7. Ozone density in the far effluent as a function of the O_2 admixture concentration. The different voltage waveforms all contain $N = 3$ consecutive harmonics, with $\phi_{pp} = 420$ V.

sawtooth waveforms produce a minimum ozone density of around 4×10^{14} cm^{-3} at 0.2% O_2 admixture, rising to a maximum ozone density of a little under 8×10^{14} cm^{-3} at 0.9% O_2. Meanwhile, peaks and valleys waveforms generate slightly higher ozone densities, with a minimum of roughly 8×10^{14} cm^{-3} at 0.4% O_2 admixture and a maximum of 1.1×10^{15} cm^{-3} and 1.0×10^{15} cm^{-3}, respectively, at 1.0% O_2. This trend and the magnitude of the ozone densities are comparable to measurements of single-frequency plasmas. This includes measurements of the plasma channel [77], where the ozone density was found to increase from around 1×10^{14} cm^{-3} to 1.2×10^{15} cm^{-3} between 0.1% and 0.9% O_2 admixture, and measurements of the early effluent [86], where

the ozone density increases from close to zero at 0.1% O_2 up to 1×10^{15} cm^{-3} at 1.0% O_2 admixture. Numerical modelling of these regions shows that ozone is primarily generated through the three-body recombination of O and O_2 with background helium [25]. It is generally accepted that this process forms ozone in a vibrationally excited state, $O_3(v)$, which is rapidly quenched by collisions with the background gas [87–89]:

$$O + O_2 + He \rightarrow O_3\left(v\right) + He \rightarrow O_3 + He. \qquad (R1)$$
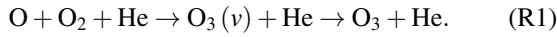
As shown by Turner [25] and Wijaikhum *et al* [77], ozone is primarily destroyed in the plasma bulk through collisions with $O_2(b^1\Sigma_u^+)$:

$$O_2\left(b^1\Sigma_u^+\right) + O_3 \rightarrow 2O_2 + O. \qquad (R2)$$
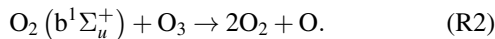
With these pathways in mind, the measured relationship between the ozone density and the concentration of O_2 is consistent with the explanation of Turner [25]. In brief, raising the O_2 admixture concentration increases the rate of ozone production via reaction (R1). This also increases the quenching rate of $O_2(b^1\Sigma_u^+)$, reducing the $O_2(b^1\Sigma_u^+)$ available to sustain reaction (R2). Thus, a higher equilibrium density of ozone is reached.

Moving to the differences between the distinct types of TVW, the two sawtooth waveforms have very similar ozone density distributions. Likewise, the ozone densities generated by the peaks and valleys waveforms are within experimental error of each other, although the measured values for the peaks waveform are slightly higher than the valleys waveform overall. A much more significant difference is found when comparing peaks and valleys waveforms with sawtooth-up and sawtooth-down waveforms. For measurements at equivalent O_2 concentrations, peaks and valleys waveforms produce an average of 1.3 times more ozone than the sawtooth waveforms.

The operational range of O_2 concentrations differs between peaks and valleys waveforms and sawtooth waveforms. This range is bounded at low O_2 concentrations by the plasma transitioning to a constricted mode, characterised by high power deposition and a high gas temperature. At high O_2 concentrations, the operational range is bounded by the plasma failing to ignite. The difference in operational range is likely caused by the time asymmetry of peaks and valleys waveforms generating stronger local electric fields than the sawtooth waveforms [58], producing electrons and helium metastables with increased efficiency and coupling more power into the plasma overall. The consequences of this phenomenon are discussed in more detail in sections 3.3 and 3.4.

These results demonstrate that the type of TVW impacts both the operational range of O_2 admixture and the density of plasma-produced ozone carried to the far effluent when the peak-to-peak driving voltage, fundamental frequency and number of applied voltage harmonics are fixed.

3.2. Influence of the peak-to-peak voltage

The peak-to-peak voltage of the driving waveform is varied to assess its influence on the RF power deposited into the plasma and the resulting ozone density measured in the far

effluent. The peaks waveform is investigated for this purpose, as its ability to break the spatial symmetry of electron heating means that it affects plasma behaviour more significantly than sawtooth waveforms [58]. Figure 8(a) shows the change in ozone density with the applied peak-to-peak voltage for peaks waveforms with $N = 1$, 2, and 4 consecutive harmonics. $N = 1$ harmonics corresponds to a sinusoidal, single-frequency voltage waveform. The $N = 2$ case is akin to conventional dual-frequency operation [48]. $N = 4$ harmonics is used instead of $N = 3$ to clearly differentiate from the dual-frequency case, while still offering a greater operational range than $N = 5$ harmonics. The O_2 admixture concentration is 0.5% in all cases. All harmonic compositions show an approximately linear increase in ozone density with peak-to-peak voltage. A minor exception is the upper voltage range of $N = 4$, where the ozone density starts to saturate.

The range of peak-to-peak voltages capable of generating a stable plasma is strongly affected by the number of applied harmonics in the driving voltage waveform. A single-frequency driving waveform allows a stable plasma to be generated with a peak-to-peak voltage in the range 380–580 V. If the driving waveform contains $N = 4$ consecutive harmonics, this range is reduced to just 115–200 V. $N = 2$, dual-frequency operation permits a similar voltage range to single-frequency use. However, using $N = 2$ harmonics allows a higher ozone density to be produced for an equivalent peak-to-peak voltage, with the difference in ozone density between dual- and single-frequency operation increasing with the peak-to-peak voltage. The highest ozone densities are produced with $N = 4$ harmonics, increasing from 3.0×10^{14} cm^{-3} to 6.4×10^{14} cm^{-3} within the operational voltage range, compared with 1×10^{13} cm^{-3} to 2.9×10^{14} cm^{-3} using single-frequency excitation. These findings are supported by data from Korolov *et al*, who showed that the atomic oxygen density in the plasma channel of a COST-Jet scaled linearly with the applied peak-to-peak voltage, and that it could be further enhanced by increasing the number of voltage harmonics in a peaks driving waveform [62]. As reaction (R1) is both the dominant mechanism for the destruction of atomic oxygen and the primary source of ozone in He+O_2 plasmas [90, 91], it follows that an increase in atomic oxygen density with peak-to-peak voltage or number of applied harmonics leads to enhanced ozone densities in the far effluent.

The relationship between the peak-to-peak voltage and the RF power deposited into the plasma is shown in figure 8(b). For all harmonic compositions, raising the peak-to-peak voltage of the driving waveform causes more RF power to be coupled into the plasma. Additionally, increasing the number of applied harmonics lowers the peak-to-peak voltage needed to achieve a given RF power deposition and reduces the maximum RF power that can be deposited into the plasma before it transitions to a constricted mode. These results agree with findings from Korolov *et al*, who found that driving a COST-Jet with a valleys waveform composed of $N = 4$ harmonics allowed a greater RF power to be deposited before the formation of the constricted mode, and for lower peak-to-peak voltages, when compared to single-frequency operation with the same fundamental frequency [61]. The power range is an order of magnitude larger in the present work, which is
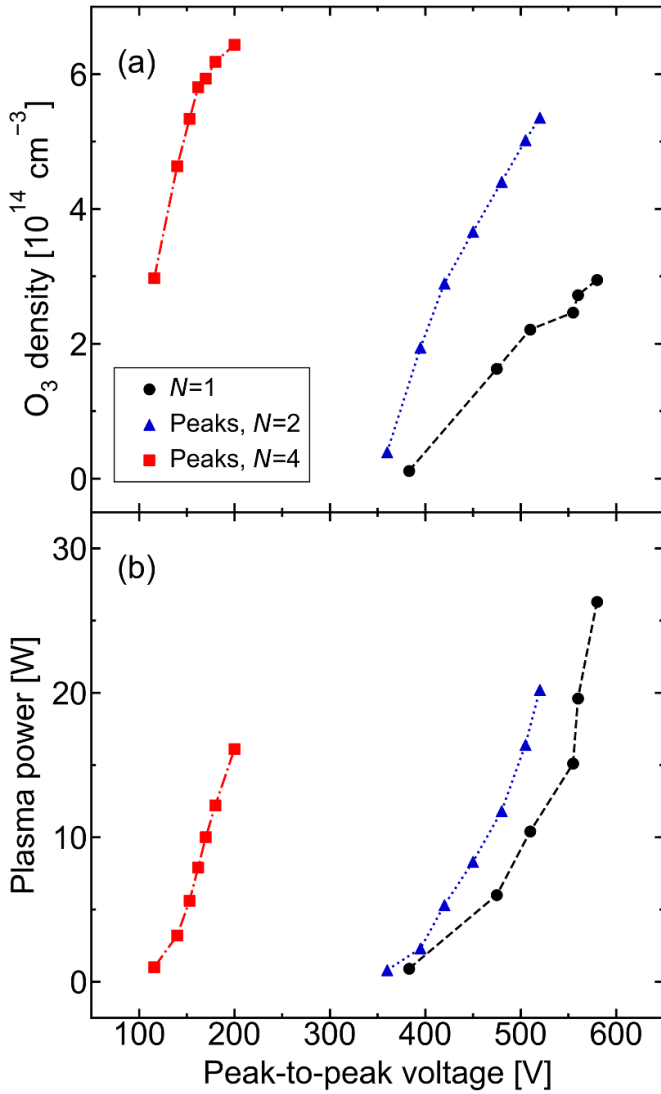
Figure 8. (a) Ozone density measured in the far effluent and (b) RF power deposited into the plasma as a function of the peak-to-peak voltage of the driving waveform, for a peaks waveform with different numbers of applied voltage harmonics. $N = 1$ denotes a sinusoidal, single-frequency waveform. The feed gas is He+O$_2$(0.5%). Characteristic measurement error in the ozone density is ±10%.

Figure 9. Ozone density measured in the far effluent as a function of the RF power deposited into the plasma. $N = 1$ denotes a sinusoidal, single-frequency waveform. The feed gas is He+O$_2$(0.5%).

attributed to our APPJ having a plasma channel volume that is approximately seven times larger than the plasma channel volume of the COST-Jet.

Figure 9 presents the ozone density as a function of the RF power deposited into the plasma.

For all harmonic compositions, raising the RF power increases the density of ozone in the effluent, although it appears to plateau with increasing RF power. Raising N also increases the density of ozone in the effluent within the operational RF power range. The overall trend between ozone density and deposited RF power agrees with ozone measurements in the far effluent of a COST-Jet by Riedel *et al*, who used a single-frequency driving waveform [92]. In contrast, measurements taken for single-frequency operation by Wijaikum *et al* show that the ozone density within the plasma channel
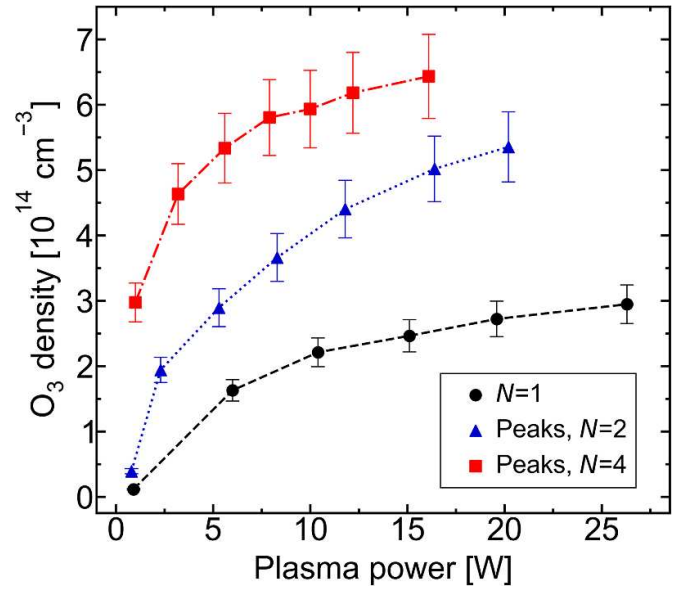
decreases as a function of deposited RF power. This was attributed to two factors. Firstly, the density of O$_2$(b$^1\Sigma_u^+$) increases with RF power, with O$_2$(b$^1\Sigma_u^+$) destroying ozone via reaction (R2) [77]. Secondly, the temperature of the background gas increases with the deposited RF power. This lowers the rate of reaction (R1), thus decreasing the production of ozone [77]. In the effluent, however, an absence of supplied power leads to a sharp decay in radical and excited species densities, and the gas temperature returns to room temperature [20, 27]. For operation with a helium carrier gas, atomic oxygen in the effluent is rapidly converted into ozone, driving an increase in the ozone density along the first few centimetres of the effluent until reaching saturation [93]. Beyond this point, the ozone density is expected to remain stable due to its long lifetime in the absence of effective reaction partners [94]. As the density of atomic oxygen scales with RF power [92], it follows that ozone production in the early effluent via reaction (R1) is responsible for the increasing ozone density seen in figure 9. The gradual saturation of the effluent ozone density is believed to result from ozone depletion in the plasma core through the mechanisms discussed above. Overall, much like with atomic oxygen, the peak-to-peak voltage or deposited RF power of TVWs can be used to control the production of ozone by an APPJ.

3.3. Influence of the applied harmonics I: constant peak-to-peak voltage

In sections 3.1 and 3.2, it has been established that the number of applied harmonics can be used in tandem with the O$_2$ admixture concentration, peak-to-peak voltage, and RF power to tailor the ozone density in the effluent of an APPJ. Fixing the peak-to-peak voltage and admixture concentration

is an often-taken approach for isolating the effects of TVW harmonics [60, 62, 95]. Here, the ozone density in the effluent, the gas temperature in the plasma channel, and the deposited RF power are investigated for different types of TVW with varying numbers of harmonics. The peak-to-peak voltage is set to $\phi_{pp} = 315$ V and the O_2 admixture concentration is 0.1%, with these values selected to maximise the range of applied harmonics that can be investigated.

The effect of the number of applied voltage harmonics on the ozone density in the far effluent is shown in figure 10(a) for different types of TVW.

Starting at $N = 2$ harmonics, the ozone density is close to 2×10^{13} cm^{-3} for the valleys and both sawtooth waveforms, and 3.7×10^{13} cm^{-3} for the peaks waveform. For the peaks and valleys waveforms, $N = 3$ is the highest number of voltage harmonics that can be applied before the plasma transitions to a constricted mode. Measurements were not performed for higher values of N due to the risk of damage to the APPJ. For the sawtooth waveforms, the ozone density increases steadily up to $N = 4$, reaching 1.4×10^{14} cm^{-3} for the sawtooth-up waveform and 1.6×10^{14} cm^{-3} for the sawtooth-down waveform. At $N = 5$ applied harmonics, the density achieved by the sawtooth-down waveform decreases to 1.3×10^{14} cm^{-3}, while for the sawtooth-up waveform it plateaus.

Detailed computational modelling by Liu *et al* suggests that the spatial density distribution of ozone in the plasma channel is not strongly affected by the symmetry-breaking effect of the valleys waveform [96]. This is because ozone is generated from interactions between neutral species and is therefore not directly affected by the electron dynamics. It is therefore reasonable to suggest that the observed enhancement of ozone densities with applied harmonics is a spatially non-localised effect that is coupled to its parent species, atomic oxygen. Atomic oxygen is primarily produced in the plasma channel through electron-impact dissociation of the O_2 admixture. This occurs either directly, or through a two-stage quenching process in which O_2 first dissociates into O and the metastable O^* [90]. It is known that increasing the number of harmonics in the driving voltage waveform enhances the high-energy tail of the EEDF, whether through temporal electron heating confinement with sawtooth waveforms or spatio-temporal electron heating confinement with peaks and valleys waveforms [58, 60]. Through this mechanism, it has been shown that the density of atomic oxygen in the plasma channel can be significantly enhanced by increasing the number of applied harmonics in a peaks waveform from $N = 1$ to $N = 4$ while maintaining a constant peak-to-peak voltage [62]. This suggests that the increase in ozone density with the number of applied harmonics results from an enhancement in atomic oxygen density that stems from localised electron heating, ultimately driving a spatially-uniform recombination of atomic oxygen into ozone in the early afterglow.

The behaviour at $N = 5$ is thought to result from the plasma becoming unstable from high RF power deposition and the deformation of the driving voltage waveform, although the plasma does not fully transition to a constricted mode. This is supported by figure 10(b), which shows the change in
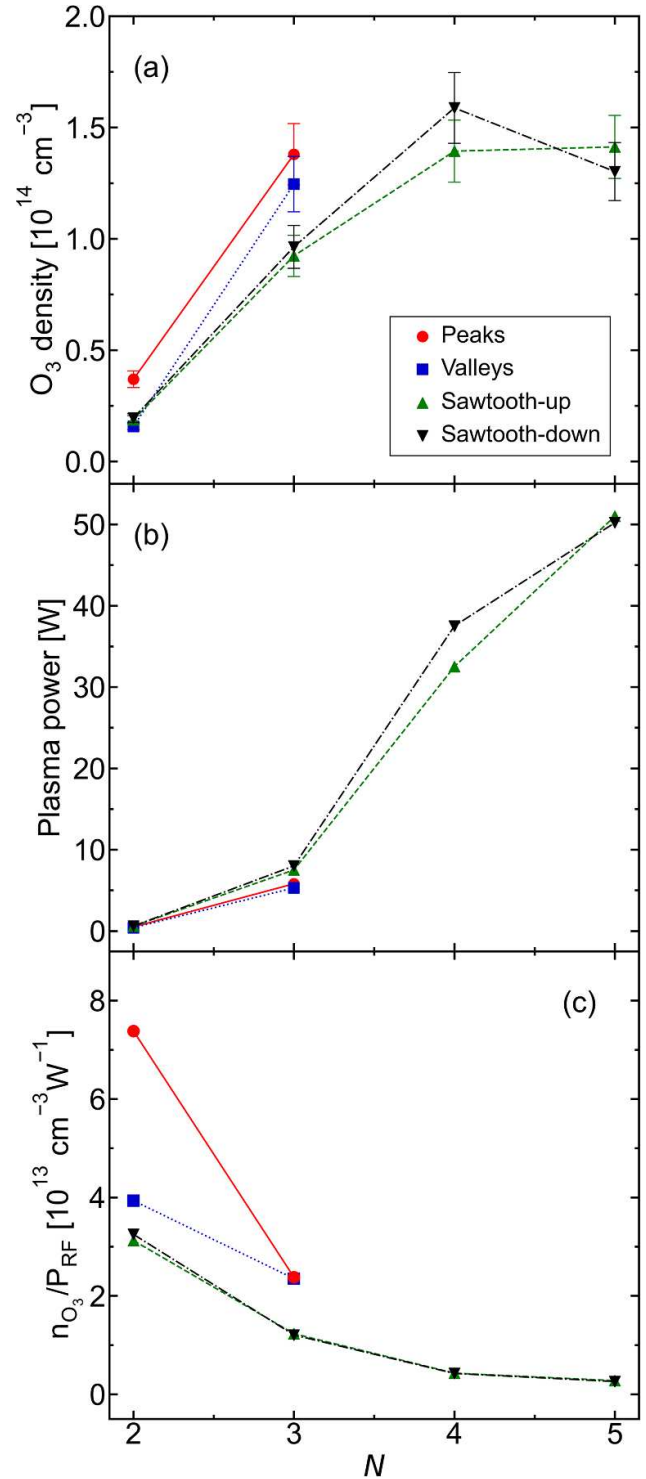
Figure 10. (a) Ozone density measured in the far effluent, (b) RF power deposited into the plasma, and (c) ozone production efficiency, as a function of the applied harmonics in the driving voltage waveform. A constant peak-to-peak voltage, $\phi_{pp} = 315$ V is used. The feed gas is He+O_2(0.1%). Plasma operation unstable for peaks and valleys waveforms when $N > 2$.

deposited RF power with the number of applied voltage harmonics. For the sawtooth waveforms, a significant increase in deposited power occurs between $N = 3$ and $N = 4$,

reaching a maximum at $N = 5$. The difference in deposited RF power between sawtooth and peaks or valleys waveforms is negligible within experimental uncertainty at both $N = 2$ and $N = 3$ applied harmonics. However, the fact that a stable plasma could not be generated with peaks and valleys waveforms for more than $N = 3$ applied harmonics suggests that these waveforms deposit appreciably more power into the plasma than sawtooth waveforms when $N > 3$. These findings align with a study by Hübner *et al*, who showed that increasing the number of applied voltage harmonics in a valleys waveform from $N = 1$ to $N = 4$ increases the power density dissipated in the plasma channel of a COST-Jet by approximately a factor of 5 for a constant peak-to-peak voltage and fundamental frequency [97]. These observations were explained by Vass *et al*. For a valleys waveform, increasing the number of applied harmonics causes stronger electron acceleration during the sheath collapse at the grounded electrode, increasing the time-averaged electron power absorption and thus the total RF power deposition [95].

Increasing the number of applied harmonics with constant peak-to-peak voltage generates energetic species, such as metastable helium, with greater efficiency [61]. However, this seemingly does not extend to ozone production as a downstream process. Normalising the measured ozone densities by the RF power deposited into the plasma, n_{O_3}/P_{RF}, provides an estimate of the efficiency of ozone production. This is shown in figure 10(c) as a function of the applied harmonics, for a constant peak-to-peak voltage. Increasing the number of applied harmonics reduces the efficiency of ozone production for all waveforms. For the sawtooth waveforms, the efficiency drops by more than one order of magnitude between $N = 2$ and $N = 5$. As such, the observed increases in ozone density with the number of applied harmonics can be explained by the overall increased power deposition achieved by these waveforms.

Figure 11 shows that the increased power coupled into the plasma is tied to a significant rise in the gas temperature within the plasma channel. For all types of TVW, the gas temperature from $N = 2$ to $N = 3$ rises no higher than 356 K. Increasing the number of applied voltage harmonics to $N = 4$ yields gas temperatures of 482 K and 514 K with the sawtooth-up and sawtooth-down waveform, respectively. A slight decrease in gas temperature is seen at $N = 5$, again attributed to the driving voltage waveform becoming unstable.

The gas temperatures observed at $N = 4$ or more applied harmonics are significantly higher than measurements from a previous study that drives the same plasma source with single-frequency voltages, which gave a typical value of around 305 K [65]. They are also much higher than the upper limits achieved in single-frequency studies of the COST-Jet [11, 20]. A similar gas heating effect was reported by Zhang *et al* in a numerical study of an atmospheric pressure, RF DBD driven by TVWs, in which the gas temperature at the centre of the reactor increased steadily with the number of applied voltage harmonics in a sawtooth-down waveform [98]. The sharp rise in gas temperature with the number of applied harmonics is likely a result of the significant power deposition causing a
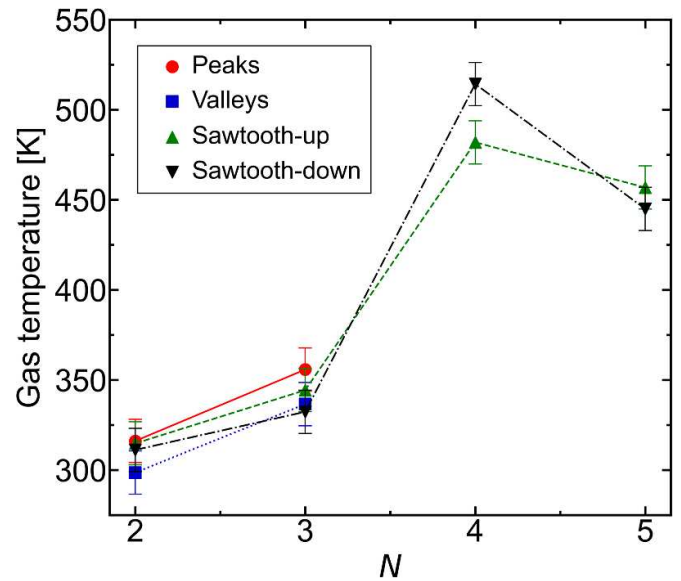
Figure 11. Gas temperature within the plasma channel as a function of the applied harmonics in the driving voltage waveform. A constant peak-to-peak voltage, $\phi_{pp} = 315\,\mathrm{V}$ is used. The feed gas is $\mathrm{He+O_2}(0.1\%)$.

sustained, localised gas heating effect by electron-neutral collisions. Operating an APPJ at these temperatures for extended periods poses a significant risk of device damage, and could potentially cause harm to biological tissues or polymer surfaces that are treated by the plasma source. The observed gas heating may also contribute to the poor ozone production efficiency seen at high numbers of applied harmonics. Ozone is sensitive to thermal decomposition and decomposes more rapidly as the gas temperature is increased, ultimately reforming O_2 [77, 99]. Moreover, the largest variation in ozone density achieved by this method is less than an order of magnitude. Similar tuning ranges are achievable with single-frequency excitation through variation of the O_2 admixture; while this requires mechanical changes that are not needed when changing the applied harmonics of a TVW, the gas temperature is consistently much lower [77].

These results demonstrate that the density of ozone in the plasma effluent can be controlled via the number of applied harmonics in the driving voltage waveform, without changing the peak-to-peak voltage. However, increasing the number of harmonics can cause significant gas heating in the plasma channel and lower the efficiency of ozone production. Despite this, it may still be possible to control ozone production through the number of applied harmonics, in a manner that is efficient and independent of the gas temperature. To explore this option, the next section investigates the use of TVWs with a fixed RF power deposition.

3.4. Influence of the applied harmonics II: constant RF power

The following measurements are taken for a constant deposited RF power of $P_{RF} = 8\,\mathrm{W}$. As such, the peak-to-peak

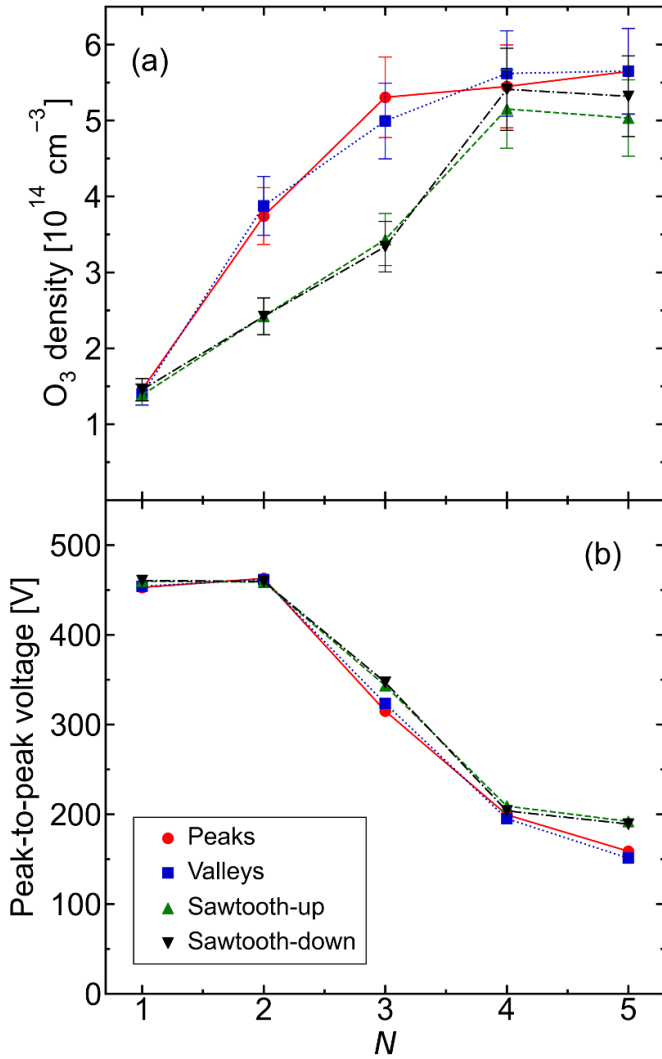**Figure 12.** (a) Ozone density measured in the far effluent and (b) the peak-to-peak voltage of the driving waveform, as a function of the number of applied harmonics. The RF power deposited in the plasma, P_{RF} is 8 W. The feed gas is He+O_2(0.5%).

voltage varies based on the voltage waveform shape and harmonic content. An O_2 admixture of 0.5% is utilised to maximise the range of operating parameters that can be compared. These operating conditions allow a stable plasma to be generated with driving voltage waveforms containing $N = 1$ to $N = 5$ applied harmonics. Figure 12(a) shows the effect of the applied voltage harmonics on the ozone density in the far effluent for a fixed RF power deposition.

The sinusoidal, $N = 1$ case generates the lowest density of ozone, at a little over 1.4×10^{14} cm^{-3}. For peaks and valleys waveforms, increasing the number of applied harmonics to $N = 3$ increases the ozone density by a factor of 3.6. The same harmonic change yields factor 2.3 and 2.5 increases for the sawtooth-up and sawtooth-down waveforms, respectively. The increase in ozone density with the number of applied harmonics for a fixed RF power deposition suggests that ozone

is being produced with increased efficiency. For an equivalent power density, Hübner *et al* found that increasing the number of applied harmonics from $N = 1$ to $N = 4$ increases the electron density, the helium metastable density, and the dissociation rate of molecular admixture within the plasma channel [97]. However, it should be noted that this is based on two sets of measurements with different fundamental frequencies. This aside, an increase in the dissociation rate of O_2 admixture would increase the ozone density in the effluent via reaction (R1). Further evidence for higher numbers of applied harmonics sustaining a more active plasma chemistry can be seen in figure 12(b), which shows the peak-to-peak voltage required to sustain the fixed RF power deposition of 8 W. Increasing the number of applied voltage harmonics above $N = 2$ allows the same RF power to be deposited into the plasma for a significantly lower peak-to-peak voltage. Raising the number of applied harmonics steepens the voltage gradients of the driving waveform, stimulating an increasingly short sheath collapse that accelerates electrons to high energies to compensate the ion flux on time average [58, 97]. This allows more power to be deposited into the plasma relative to the peak-to-peak voltage of the driving waveform.

As discussed in section 1, different types of TVW exert different symmetry-breaking effects on the plasma; electron heating is confined only in time by sawtooth waveforms, while peaks and valleys waveforms restrict electron heating in both time and space [58]. This improved localisation of power transfer enables peaks and valleys waveforms to drive a more efficient production of atomic oxygen than the sawtooth waveforms, with its recombination resulting in the greater ozone densities generated with peaks and valleys waveforms at $N = 2$ and $N = 3$ when compared to the sawtooth waveforms. Interestingly, all four waveforms appear to reach a similar upper limit in the ozone density at $N = 4$ applied voltage harmonics, with negligible change seen if N is increased to 5. While the physical cause of this limit is unclear, it is feasible that increasing the number of applied harmonics enhances the ozone density until an upper threshold is reached. Referring to the model TVWs in figure 2, as the number of applied harmonics rises, the relative change in the voltage gradient between consecutive harmonics decreases, as does the relative change in the duration of periods of high voltage gradient. Furthermore, increasing the number of harmonics also decreases the relative change in the asymmetrical displacement of peaks and valleys waveforms along the voltage axis, although this last effect may differ in practice due to the formation of a DC self-bias voltage [59]. The progressively decreasing relative change in these parameters may lead to a 'diminishing returns' effect at high numbers of harmonics. In this case, electron heating cannot be further restricted in time or space in a way that would noticeably affect the plasma chemistry, nor can the strong electric field generated by the voltage slope be appreciably increased. This would limit the degree to which the high-energy tail of the EEDF can be enhanced, in turn limiting the production of atomic oxygen through electron-impact dissociation of O_2 and creating
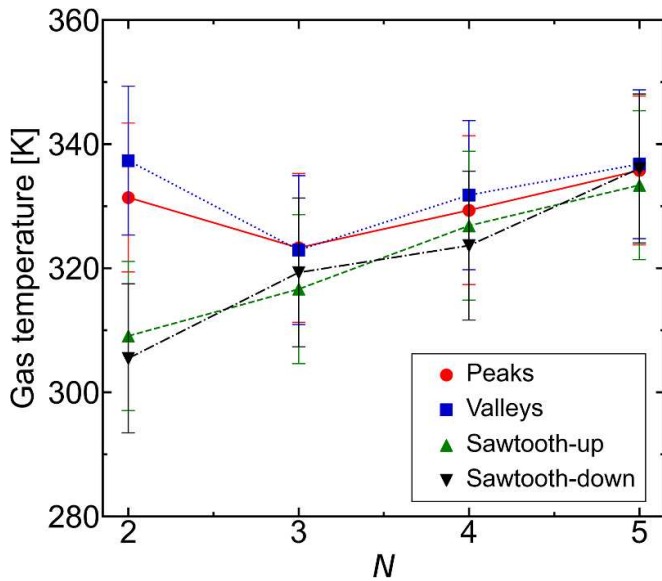
Figure 13. Time-averaged gas temperature within the plasma channel as a function of the number of applied harmonics in the driving voltage waveform. The RF power deposited in the plasma, P_{RF} is 8 W. The feed gas is He+O_2(0.5%).

an upper threshold in the density of ozone produced through the recombination of atomic oxygen. This is beyond the scope of the present study; it remains for future works to investigate a possible upper limit to atomic oxygen production with TVWs.

Figure 13 shows the change in the gas temperature of the plasma channel with the number of applied harmonics for a fixed RF power deposition. Tuning between $N = 2$ and $N = 5$ applied voltage harmonics with constant RF power results in a much lower change in the gas temperature of the plasma channel when compared to operation with a constant peak-to-peak voltage, with the temperature change almost negligible outside of the experimental uncertainty. The measured gas temperature does not exceed 340 K, and a minimum gas temperature of 305 K is obtained by using a sawtooth-down waveform with $N = 2$ applied harmonics. Evidently, operation with a fixed RF power deposition prevents excessive gas heating while still allowing the density of ozone to be controlled and the efficiency of ozone production to be increased. Kelly *et al* previously reported that, depending on the peak-to-peak voltage and gas flow rate, a COST-Jet driven with a single-frequency voltage waveform could be operated stably in the Ω-mode with a peak gas temperature of up to approximately 380 K at the end of the plasma channel [20]. Likewise, Golda *et al* measured the gas temperature at a distance of 3 mm along the effluent of a COST-Jet and presented a maximum gas temperature of roughly 350 K at the highest RF power investigated [11]. These readings are larger than the gas temperatures presented in figure 13, indicating that the APPJ can be safely operated in this temperature range. It can therefore be concluded that fixing the RF power deposition allows the ozone density to be tailored through the number of applied voltage harmonics, while maintaining a relatively low gas temperature within the plasma channel.

4. Conclusion

RF, APPJs are efficient sources of RONS. Controlling the production of these species is an essential step in optimising the application of plasma jets in industry. This work presents the first investigation into the effects of TVWs on long-lived reactive species carried through the effluent of an APPJ. A plasma is generated from a helium feed gas with small admixtures of O_2, driven by TVWs composed of up to five consecutive voltage harmonics with a fundamental frequency of 13.56 MHz. The density of ozone in the far effluent is measured by FTIR spectroscopy and the gas temperature in the plasma channel is determined by OES. Driving a plasma with a peaks waveform is found to increase the density of ozone in the effluent when compared to single-frequency operation, with the density of ozone increasing with the number of harmonics. Peaks and valleys waveforms are found to generate more ozone than sawtooth waveforms under equivalent conditions. For a fixed peak-to-peak voltage, increasing the number of harmonics enhances the ozone density but significantly increases the gas temperature within the plasma channel due to rising RF power deposition. Efficient control of the ozone density is instead achieved by changing the number of applied harmonics for a fixed RF power deposition. This allows the ozone density to be enhanced without appreciably changing the gas temperature in the plasma channel. The results highlight that TVWs can be used to control the ozone density in the plasma effluent, offering more methods of control than with single-frequency voltage waveforms, which is essential to realise the potential of these devices in real-world applications.

Data availability statement

The data that support the findings of this study are openly available at the following URL/DOI: https://doi.org/10.15124/8f592a52-ba89-4271-baaf-1d45b6cf4fea.

Acknowledgments

ORCID iDs

Benjamin Harris ⬥ https://orcid.org/0000-0002-4036-8585
James P Dedrick ⬥ https://orcid.org/0000-0003-4353-104X
Kari Niemi ⬥ https://orcid.org/0000-0001-6134-1974
Erik Wagenaars ⬥ https://orcid.org/0000-0002-5493-3434

References

[1] Adamovich I *et al* 2022 *J. Phys. D: Appl. Phys.* **55** 373001
[2] Graves D B 2012 *J. Phys. D: Appl. Phys.* **45** 263001
[3] West A, van der Schans M, Xu C, Cooke M and Wagenaars E 2016 *Plasma Sources Sci. Technol.* **25** 02LT01
[4] Shaw D, West A, Bredin J and Wagenaars E 2016 *Plasma Sources Sci. Technol.* **25** 065018

[5] Brandenburg R *et al* 2019 *Plasma Process. Polym.* **16** 1700238

[6] Lu X, Laroussi M and Puech V 2012 *Plasma Sources Sci. Technol.* **21** 034005

[7] Von Woedtke T, Reuter S, Masur K and Weltmann K D 2013 *Phys. Rep.* **530** 291–320

[8] Lu X, Naidis G, Laroussi M a and Ostrikov K 2014 *Phys. Rep.* **540** 123–66

[9] Schutze A, Jeong J Y, Babayan S E, Park J, Selwyn G S and Hicks R F 1998 *IEEE Trans. Plasma Sci.* **26** 1685–94

[10] Schulz-von der G V, Buck V, Gans T, Knake N, Niemi K, Reuter S, Schaper L and Winter J 2007 *Contrib. Plasma Phys.* **47** 510–9

[11] Golda J *et al* 2016 *J. Phys. D: Appl. Phys.* **49** 084003

[12] Laroussi M and Lu X 2005 *Appl. Phys. Lett.* **87** 113902

[13] Setsuhara Y 2016 *Arch. Biochem. Biophys.* **605** 3–10

[14] Gorbanev Y, Golda J, Schulz-von der G V and Bogaerts A 2019 *Plasma* **2** 316–27

[15] Harris B, Krös L, Nave A, Wagenaars E and van Helden J 2023 *Plasma Sources Sci. Technol.* **32** 115010

[16] Elvis A and Ekta J 2011 *J. Nat. Sci. Biol. Med.* **2** 66

[17] Kim J G, Yousef A E and Khadre M A 2003 *Adv. Food Nutrition Res.* **45** 167–218

[18] Kogelschatz U 2003 *Plasma Chem. Plasma Process.* **23** 1–46

[19] Takeuchi N and Yasuoka K 2020 *Jpn. J. Appl. Phys.* **60** SA0801

[20] Kelly S, Golda J, Turner M M and Schulz-von der G V 2015 *J. Phys. D: Appl. Phys.* **48** 444002

[21] Wagenaars E, Gans T, O'Connell D and Niemi K 2012 *Plasma Sources Sci. Technol.* **21** 042002

[22] Niemi K, O'Connell D, de Oliveira N, Joyeux D, Nahon L, Booth J P and Gans T 2013 *Appl. Phys. Lett.* **103** 034102

[23] Liu K, Geng W, Zhou X, Duan Q, Zheng Z and Ostrikov K K 2023 *Plasma Sources Sci. Technol.* **32** 025005

[24] Sousa J S, Niemi K, Cox L, Algwari Q T, Gans T and O'connell D 2011 *J. Appl. Phys.* **109** 123302

[25] Turner M M 2015 *Plasma Sources Sci. Technol.* **24** 035027

[26] Murakami T, Niemi K, Gans T, O'Connell D and Graham W G 2012 *Plasma Sources Sci. Technol.* **22** 015003

[27] Murakami T, Niemi K, Gans T, O'Connell D and Graham W G 2014 *Plasma Sources Sci. Technol.* **23** 025005

[28] Brisset A, Gibson A R, Schröter S, Niemi K, Booth J P, Gans T, O'Connell D and Wagenaars E 2021 *J. Phys. D: Appl. Phys.* **54** 285201

[29] Brisset A, Harris B, Dickenson A, Niemi K, Walsh J and Wagenaars E 2022 *Plasma Sources Sci. Technol.* **31** 045008

[30] Brisset A, Bieniek M, Invernizzi L, Hasan M, Walsh J, Niemi K and Wagenaars E 2023 *Plasma Sources Sci. Technol.* **32** 065004

[31] Harris B and Wagenaars E 2023 *J. Appl. Phys.* **134** 103302

[32] Hemke T, Eremin D, Mussenbrock T, Derzsi A, Donkó Z, Dittmann K, Meichsner J and Schulze J 2012 *Plasma Sources Sci. Technol.* **22** 015012

[33] Bischoff L *et al* 2018 *Plasma Sources Sci. Technol.* **27** 125009

[34] Schulz-Von D G V, Schaper L, Knake N, Reuter S, Niemi K, Gans T and Winter J 2008 *J. Phys. D: Appl. Phys.* **41** 194004

[35] Liu Y, Korolov I, Hemke T, Bischoff L, Hübner G, Schulze J and Mussenbrock T 2021 *J. Phys. D: Appl. Phys.* **54** 275204

[36] Schröder D, Burhenn S, De los Arcos T and Schulz-von der G V 2015 *J. Phys. D: Appl. Phys.* **48** 055206

[37] Iza F, Lee J K and Kong M G 2007 *Phys. Rev. Lett.* **99** 075004

[38] Niemi K, Waskoenig J, Sadeghi N, Gans T and O'Connell D 2011 *Plasma Sources Sci. Technol.* **20** 055005

[39] Golda J, Kogelheide F, Awakowicz P and Schulz-von der G V 2019 *Plasma Sources Sci. Technol.* **28** 095023

[40] Mouchtouris S, Kokkoris G and Boudouvis A G 2022 *J. Phys. D: Appl. Phys.* **55** 355203

[41] Goto H H, Löwe H D and Ohmi T 1992 *J. Vac. Sci. Technol.* A **10** 3048–54

[42] Kitajima T, Takeo Y, Petrović Z L and Makabe T 2000 *Appl. Phys. Lett.* **77** 489–91

[43] Boyle P, Ellingboe A and Turner M 2004 *J. Phys. D: Appl. Phys.* **37** 697

[44] Schulze J, Gans T, O'Connell D, Czarnetzki U, Ellingboe A and Turner M 2007 *J. Phys. D: Appl. Phys.* **40** 7008

[45] O'Connell D, Gans T, Semmler E and Awakowicz P 2008 *Appl. Phys. Lett.* **93** 081502

[46] Waskoenig J and Gans T 2010 *Appl. Phys. Lett.* **96** 181501

[47] Kim D B, Moon S Y, Jung H, Gweon B and Choe W 2010 *Phys. Plasmas* **17** 053508

[48] O'Neill C, Waskoenig J and Gans T 2012 *Appl. Phys. Lett.* **101** 154107

[49] Zhou Y J, Yuan Q H, Li F, Wang X M, Yin G Q and Dong C Z 2013 *Phys. Plasmas* **20** 113502

[50] Zhang Z, Nie Q, Wang Z, Gao X, Kong F, Sun Y and Jiang B 2016 *Phys. Plasmas* **23** 073501

[51] Heil B G, Czarnetzki U, Brinkmann R P and Mussenbrock T 2008 *J. Phys. D: Appl. Phys.* **41** 165202

[52] Donkó Z, Schulze J, Heil B and Czarnetzki U 2008 *J. Phys. D: Appl. Phys.* **42** 025205

[53] Schulze J, Schüngel E, Donkó Z and Czarnetzki U 2011 *Plasma Sources Sci. Technol.* **20** 015017

[54] Lafleur T, Delattre P A, Johnson E and Booth J P 2012 *Appl. Phys. Lett.* **101** 124104

[55] Lafleur T 2015 *Plasma Sources Sci. Technol.* **25** 013001

[56] Doyle S J, Gibson A R, Boswell R W, Charles C and Dedrick J P 2020 *Plasma Sources Sci. Technol.* **29** 124002

[57] Derzsi A, Bruneau B, Gibson A R, Johnson E, O'Connell D, Gans T, Booth J P and Donkó Z 2017 *Plasma Sources Sci. Technol.* **26** 034002

[58] Gibson A R *et al* 2019 *Plasma Sources Sci. Technol.* **28** 01LT01

[59] Korolov I, Donko Z, Hübner G, Bischoff L, Hartmann P, Gans T, Liu Y, Mussenbrock T and Schulze J 2019 *Plasma Sources Sci. Technol.* **28** 094001

[60] Korolov I *et al* 2020 *J. Phys. D: Appl. Phys.* **53** 185201

[61] Korolov I, Donkó Z, Hübner G, Liu Y, Mussenbrock T and Schulze J 2021 *Plasma Sources Sci. Technol.* **30** 095013

[62] Korolov I, Steuer D, Bischoff L, Hübner G, Liu Y, Schulz-Von der Gathen V, Böke M, Mussenbrock T and Schulze J 2021 *J. Phys. D: Appl. Phys.* **54** 125203

[63] Mouele E S M *et al* 2021 *J. Environ. Chem. Eng.* **9** 105758

[64] Dedrick J, Schröter S, Niemi K, Wijaikhum A, Wagenaars E, de Oliveira N, Nahon L, Booth J P, O'Connell D and Gans T 2017 *J. Phys. D: Appl. Phys.* **50** 455204

[65] Schröter S *et al* 2018 *Phys. Chem. Chem. Phys.* **20** 24263–86

[66] Nahon L, de Oliveira N, Garcia G A, Gil J F, Pilette B, Marcouillé O, Lagarde B and Polack F 2012 *J. Synchrotron Radiat.* **19** 508–20

[67] Derzsi A, Lafleur T, Booth J P, Korolov I and Donkó Z 2015 *Plasma Sources Sci. Technol.* **25** 015004

[68] Bruneau B, Novikova T, Lafleur T, Booth J P and Johnson E 2014 *Plasma Sources Sci. Technol.* **23** 065010

[69] Lafleur T, Delattre P A, Booth J, Johnson E and Diné S 2013 *Rev. Sci. Instrum.* **84** 015001

[70] Horwitz C M 1983 *J. Vac. Sci. Technol.* A **1** 1795–800

[71] McCaa D and Shaw J 1968 *J. Mol. Spectrosc.* **25** 374–97

[72] Barbe A, Mikhailenko S, Starikova E and Tyuterev V 2022 *Molecules* **27** 911

[73] Gordon I E *et al* 2022 *J. Quant. Spectrosc. Radiat. Transfer* **277** 107949

[74] Wang Q, Doll F, Donnelly V M, Economou D J, Sadeghi N and Franz G F 2007 *J. Phys. D: Appl. Phys.* **40** 4202

[75] Wang Q, Koleva I, Donnelly V M and Economou D J 2005 *J. Phys. D: Appl. Phys.* **38** 1690

[76] Bruggeman P J, Sadeghi N, Schram D and Linss V 2014 *Plasma Sources Sci. Technol.* **23** 023001

[77] Wijaikhum A, Schröder D, Schröter S, Gibson A R, Niemi K, Friderich J, Greb A, Schulz-von der G V, O'Connell D and Gans T 2017 *Plasma Sources Sci. Technol.* **26** 115004

[78] Niemi K, Reuter S, Graham L, Waskoenig J, Knake N, Schulz-Von D G V and Gans T 2010 *J. Phys. D: Appl. Phys.* **43** 124006

[79] Nwankire C E, Law V J, Nindrayog A, Twomey B, Niemi K, Milosavljević V, Graham W and Dowling D 2010 *Plasma Chem. Plasma Process.* **30** 537–52

[80] Twomey B, Nindrayog A, Niemi K, Graham W and Dowling D 2011 *Plasma Chem. Plasma Process.* **31** 139–56

[81] Meehan D N, Niemi K and Wagenaars E 2020 *Jpn. J. Appl. Phys.* **59** SHHB03

[82] Herzberg G 1945 *Molecular Spectra and Molecular Structure* (D. van Nostrand)

[83] Roux F, Michaud F and Vervloet M 1993 *J. Mol. Spectrosc.* **158** 270–7

[84] Kovács I 1966 *Astrophys. J.* **145** 634

[85] Schadee A 1975 *Astron. Astrophys.* **41** 203

[86] Ellerweg D, Benedikt J, von Keudell A, Knake N and Schulz-von der G V 2010 *New J. Phys.* **12** 013021

[87] von Rosenberg C Jr and Trainor D W 1973 *J. Chem. Phys.* **59** 2142–2142

[88] Lopaev D, Malykhin E and Zyryanov S 2010 *J. Phys. D: Appl. Phys.* **44** 015202

[89] Booth J P, Guaitella O, Zhang S, Lopaev D, Zyryanov S, Rakhimova T, Voloshin D, Chukalovsky A, Volynets A and Mankelevich Y 2023 *Plasma Sources Sci. Technol.* **32** 095016

[90] Waskoenig J, Niemi K, Knake N, Graham L, Reuter S, Schulz-Von D G V and Gans T 2010 *Plasma Sources Sci. Technol.* **19** 045018

[91] Turner M M 2016 *Plasma Sources Sci. Technol.* **25** 015003

[92] Riedel F, Golda J, Held J, Davies H, van der Woude M, Bredin J, Niemi K, Gans T, Schulz-von der G V and O'Connell D 2020 *Plasma Sources Sci. Technol.* **29** 095018

[93] Ellerweg D, Von Keudell A and Benedikt J 2012 *Plasma Sources Sci. Technol.* **21** 034019

[94] McClurkin J D, Maier D E and Ileleji K E 2013 *J. Stored Prod. Res.* **55** 41–47

[95] Vass M, Wilczek S, Schulze J and Donkó Z 2021 *Plasma Sources Sci. Technol.* **30** 105010

[96] Liu Y, Korolov I, Trieschmann J, Steuer D, Schulz-von der G V, Böke M, Bischoff L, Hübner G, Schulze J and Mussenbrock T 2021 *Plasma Sources Sci. Technol.* **30** 064001

[97] Hübner G, Bischoff L, Korolov I, Donkó Z, Leimkühler M, Liu Y, Böke M, Schulz-von der G V, Mussenbrock T and Schulze J 2021 *J. Phys. D: Appl. Phys.* **55** 095204

[98] Zhang Z, Nie Q, Zhang X, Wang Z, Kong F, Jiang B and Lim J 2018 *Phys. Plasmas* **25** 043502

[99] Benson S W and Axworthy A E Jr 1957 *J. Chem. Phys.* **26** 1718–26